

On the Performance of Pilot-Aided Simultaneous Communication and Tracking

Shuaishuai Han, *Student Member, IEEE*, Emad Alsusa, *Senior Member, IEEE*, Mohammad Ahmad Al-Jarrah, *Member, IEEE*, Mahmoud AlaaEldin, *Member, IEEE*,

Abstract—In this paper, the symbol error rate performance analysis is provided for a pilot-aided simultaneous communication and tracking (PASCAT) system. In specific, we employ multiple drones to actively transmit signals to a BS, which is responsible for continuously monitoring the location of drones over time and decoding the symbols transmitted from the drones. It is found that the estimated location parameters at a given moment during tracking follow Gaussian distributions with means equal to actual values and variances equal to root mean square error (RMSE). Afterwards, the obtained location information is employed for informing the channel information, which is then used to preprocess the received signal before decoding by using the maximum ratio combining (MRC) technique. The average symbol error rate (SER) is also evaluated over the distribution of the estimated location parameters and an approximate value for the average SER is obtained by using a Taylor approximation with fast convergence. The result indicates that there is a cooperation relationship between the RMSE of the estimated location parameters and the average SER. In addition, the effect of the number of pilot signals is analysed as well. By employing more pilots, it is found that both communication and sensing functionalities are enhanced. Furthermore, the SER performance of our PASCAT system is similar to that of maximum likelihood detection (MLD) when a number of pilot signals are employed, which demonstrates the efficiency of the PASCAT system. In the end, all results are validated by using Monte Carlo simulations.

Index Terms—Symbol error rate (SER), performance analysis, pilot-aided simultaneous communication and tracking (PASCAT), root mean square error (RMSE), maximum likelihood detection (MLD)

I. INTRODUCTION

With the commercial deployment of the fifth generation (5G) mobile communication systems worldwide, research on beyond 5G and the sixth generation (6G) has been advancing rapidly. Among the various emerging technologies, integrated sensing and communication (ISAC) has been considered an essential technique for next-generation wireless networks such as beyond 5G and 6G due to the fact that it allows both sensing and communication functions to be conducted in the same platform by sharing the same network resources and signal-processing modules [1]. As a consequence, compared to traditionally separated sensing and communication systems, ISAC has obtained obvious advantages in the efficiency of spectrum, energy, and

hardware. However, the majority of current research on ISAC ignores the fact that the targets to be localised such as drones can have their own transceivers. These kinds of targets can actively transmit signals to the base station (BS) not only to communicate with the BS but also to enable localisation or tracking with the assistance of pilot signals. As a consequence, we introduce the pilot-aided simultaneous communication and tracking (PASCAT) system. Compared to the ISAC system, PASCAT is superior in energy efficiency as it only suffers from one-way path loss. On the contrary, the existing ISAC system [2–5] typically transmits signals to the targets and relies on the echos for localisation, resulting in higher energy consumption.

Channel estimation plays an essential role in the communication system since the signal transmission rate and error rate both highly rely on the accuracy of channel state information (CSI). Interestingly, by acknowledging that location information contributes a significant portion of CSI, especially in the line of sight (LOS) case, we can leverage localisation or tracking results to boost communication performance. This method of acquiring channel information is referred to as parametric channel estimation, which has been proven in [6] to provide more accurate CSI by employing fewer pilot signals than non-parametric estimation, where the channel is estimated as a whole. Furthermore, parametric channel estimation is more suitable than non-parametric one to be employed in the PASCAT system as the system inherently requires the estimation of location information, which can then be effectively utilised for obtaining the channel information. As a consequence, parametric channel estimation is considered in this paper.

A. Integrated Sensing and Communication

In the past few years, there has been growing interest in ISAC techniques since ISAC offers substantial benefits from sharing spectrum and equipment while ensuring non-interference between the communication and sensing systems compared to separate designs. Nevertheless, although many studies have implemented communication and sensing functionalities on the same platform, these functionalities are applied to different objects separately. In this way, the obtained location information is not employed to assist the communication function. For instance, the authors of [7, 8] employ a radar-communications BS with the collocated transmit array and receive array, in which, the transmit array is responsible for transmitting sensing signals to targets to be localised, while the receive array is employed to receive both the echos reflected from the targets for sensing and process the signals coming from the users for uplink

Shuaishuai Han, E. Alsusa, M. A. Al-Jarrah and Mahmoud AlaaEldin are with the Department of Electrical and Electronic Engineering, University of Manchester, Manchester M13 9PL, U.K. (e-mail: shuaishuai.han@postgrad.manchester.ac.uk, {e.alsusa, mohammad.al-jarrah, mahmoud.alaaeldin}@manchester.ac.uk).

communication. In [9–12], an ISAC BS is employed to perform downlink communication with users and localises the targets at the same time by transmitting sensing signals and receiving the reflected signals. In [13], the authors employ the BS to transmit ISAC signals to communicate with multiple vehicles and also receive echoes to track the locations of the same vehicles. However, they still ignore the substantial potential of localisation results in enhancing the performance of communication. As a consequence, the estimated location information by the BS in the aforementioned research has not been efficiently utilized.

B. Performance Analysis for ISAC

With the growing interest in the ISAC technique, an increasing amount of research is focusing on the performance analysis of ISAC, such as the trade-off analysis. In [14], Cramér-Rao bound (CRB)-communication rate analysis is provided to depict the fundamental sensing and communication trade-off, where CRB is employed as a lower bound for evaluating the sensing performance. In [15], the trade-off between probability of coverage and probability of detection is explored under power or bandwidth allocation, in which probability of coverage and probability of detection are employed for evaluating the communication and localisation systems, respectively. In [16], the trade-off between radar imaging error and channel capacity is analysed. Such trade-off analysis is beneficial for understanding the interaction between sensing and communication functionalities (e.g., competitive), while providing guidance for developing efficient algorithms or techniques. However, the aforementioned analysis focuses on the competitive relationship between communication and sensing functions given a limited amount of power and bandwidth, few studies take the potential mutual cooperation relationship into account. In specific, the localisation result may directly influence the communication performance, and thus an improved localisation accuracy can enhance the communication performance.

C. Localisation and Tracking

The implementation of sensing in the ISAC research includes, but is not limited to, the localisation and tracking of the targets. The localisation in ISAC can be completed with the assistance of pilot signals. In [17], the pilot signal is inserted into the data frame for estimating the Doppler frequency information. In [18], the BS transmits pilot signals to obtain an initial search for target locations. Employing pilot signals enables the acquisition of important location information before data decoding. Compared to localisation, tracking is more general as it can continuously monitor the positions of targets over time instead of estimating their positions at a given moment. Many studies on tracking are based on Kalman filter (KF) or Extended Kalman Filter (EKF), for instance, [19, 20]. The High-precision tracking performance brought by KF and EKF has already been demonstrated in these studies. Nonetheless, these studies achieve tracking by using the reflected signal from the targets and thus this kind of tracking suffers from two-way path loss. To guarantee the signal strength of the received signal, the transmitter has to increase the transmit energy, which results in energy inefficiency.

D. Motivation and Contributions

Motivated by the fact that there is an urgent requirement to develop a more energy-efficient system than the conventional ISAC systems which employ the reflected signals for sensing and most of the current ISAC research ignores the potential cooperation relationship between sensing and communication functionalities, we introduce a PASCAT system in this paper. It is worth mentioning that tracking in this paper is completed by continuously estimating the locations of drones instead of using KF since the KF scheme assumes the locations and velocities of drones to be random and follow the Gaussian distribution, which may increase the complexity of performance analysis significantly. Compared to the tracking system in [19, 20], the proposed PASCAT system employs multiple drones to actively transmit signals to a ground BS, which is responsible for both tracking the drones by using pilot signals and decoding the symbols transmitted from the drones. As a result, PASCAT only suffers from one-way path loss instead of two-way path loss. In addition, the estimated location information is employed to provide CSI (e.g., parametric channel estimation), which is then utilised to preprocess the received signal to enhance the signal quality. Meanwhile, we adopt an increasing number of pilot signals to improve the localisation performance, which results in more accurate CSI and enhanced communication performance. Thus the communication functionality can benefit from the localisation results. Our main contributions can be summarised as follows.

- 1) We propose a PASCAT system that employs drones to actively send signals to a BS, where the latter tracks the drones with an increasing number of pilot signals and communicates with the drones.
- 2) The statistical characteristic of the estimated location parameters at a given moment with Gaussian noise is analysed. We find that the estimated location parameters follow independent Gaussian distributions with variances equal to root mean square error (RMSE). Thereafter, the estimated location parameters are employed for obtaining the channel information, which is then utilised to preprocess the received signal with the maximum ratio combining (MRC) technique.
- 3) The symbol error rate (SER) analysis is provided to evaluate the influence of the estimation errors for location parameters on the decoding performance. The SER analysis based on such parametric channel estimation is different from that of the conventional non-parametric one, such as [21, 22] since the channel information in the former is obtained by directly using the estimated location parameters instead of estimating the channel as a whole. Thus, it is more difficult to understand the overall distribution of the channel. Moreover, the estimated channels of different antennas share the same estimated location parameters, which results in a high correlation between the estimated channels belonging to different antennas. To solve this, a conditional SER given the estimation errors of location parameters is derived first, which is then evaluated over

the distributions of the estimation errors to obtain the average SER by using a Taylor approximation with fast convergence.

- 4) To evaluate the performance of the developed PASCAT system, simulation and analytical results are provided. The results indicate that the increase in pilot numbers affects both communication and tracking functionalities in the PASCAT system. In addition, there is a cooperation relationship between the RMSE of the estimated location parameters and the SER, and the analytical SER is a function of the RMSE. It is also found that the SER performance of our PASCAT system is comparable to that of maximum likelihood detection (MLD) when a number of pilots are available. In the end, the analytical and simulation results match perfectly with limited Taylor approximation orders.

The rest of the paper is organised as follows. In Sec. II, the system model for the proposed PASCAT system is provided. Sec. III illustrates the maximum likelihood (ML) based tracking algorithm and data detection with MRC. Sec. IV presents the performance analysis for evaluating the communication and tracking performance of the PASCAT system. Sec. V demonstrates the simulation and analytical results, and Sec. VI concludes this paper.

Notations: $\hat{\mathbf{p}}$ denotes a vector composed of estimated parameters. $\|\cdot\|_2$ represents the Euclidean norm. $\mathbb{E}[\cdot]$ refers to the statistical expectation. $\det(\cdot)$ represents the determinant of a matrix. $[\cdot]^*$, $[\cdot]^T$ and $[\cdot]^H$ indicates the complex conjugate, transposition and Hermitian transposition.

II. SYSTEM MODEL

In PASCAL, we consider a multiuser single-input multiple-output (MU-SIMO) system employing K moving single-antenna drones located in the far field to send information signals to a BS composed of multiple antennas, where the latter aims to track the drones and decode symbols with the pilot signals. The above system model is applicable to scenarios such as Global Positioning System (GPS)-denied environments [23] including tunnel, forest and underground environments where the precise GPS information of the drones is not available. Furthermore, commercial GPS may not be accurate in tracking drones. For instance, the estimation errors for the altitude of the drones could reach 15 m. Such amount of error is considerable especially when the density of deployed drones is high and could lead to drones' clashes under these circumstances. As a consequence, the drones in the PASCAL system are employed to actively send information signals to the BS to allow the latter to leverage these signals to complete the tracking of the drones. Due to the fact that the likelihood of Line-of-Sight (LOS) channel availability in air-to-ground (A2G) links is high and undesired Non-LOS (NLOS) paths shown in radar images could affect the reliable identification of the targets in the MIMO radar-based localisation, which is referred to as the virtual or ghost targets phenomenon [24], we employ ray tracing [25] to pre-process the received signal and extract the LOS component from the multi-path components before localisation, as shown in

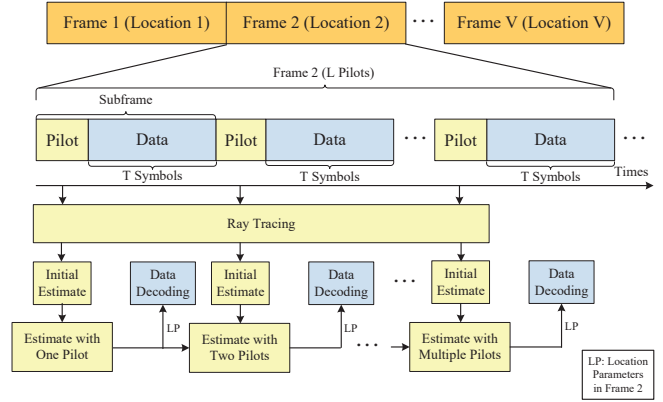


Fig. 1. Frame structure for the PASCAT system.

Fig. 1.

Once the information signals are received by the BS, it will decode the symbols and extract the location information including direction of arrival (DOA), range and Doppler frequency from the information signals. The DOA, range and Doppler frequency of drone k can be denoted by using θ_k , d_k and $f_{D,k}$, which are unknown constants. It is worth noting Doppler frequency is employed in this paper to denote the velocity of drones. Since the velocities and locations of the drones may remain constant for a short period, θ_k , d_k and $f_{D,k}$ for $k \in \{1, \dots, K\}$ can be assumed to be time-invariant during each frame, which is similar to the assumption used in [26]. This assumption is reasonable as, for instance, a frame with a length of 1000 symbols only takes up 1×10^{-3} seconds when the symbol rate is 10^6 symbols per second. Thereafter, the tracking of the drones is accomplished by estimating and collecting the location information of drones in each frame, until the trajectory of the drones over multiple frames is obtained. It is worth mentioning that no prediction of drones is considered to simplify the analysis in this paper, which is similar to the tracking process of the ISAC paper [27]. The BS used in this paper is composed of a uniform linear array (ULA) with N antennas, where every two adjacent antennas are separated with a distance of half of the wavelength, i.e., $d = \lambda/2$.

The frame structure is shown in Fig. 1, in which there are L subframes in each frame and each subframe is composed of a pilot signal and T signals with symbol. By arranging the outputs of the matched filter, the received signal vector for the t th signal within the l th subframe at the BS from all the drones, in which $t \in \{0, \dots, T\}$ and $l \in \{1, \dots, L\}$, can be denoted by

$$\mathbf{y}_{t,l} = \mathbf{A}\boldsymbol{\omega}(l)\mathbf{s}_{t,l} + \mathbf{n}, \quad (1)$$

where $\mathbf{y}_{t,l} \in \mathbb{C}^{N \times 1}$ contains the signals received by the N antennas of the BS and $\mathbf{A}\boldsymbol{\omega}(l) \in \mathbb{C}^{N \times K}$ indicates the LOS channel response. $\mathbf{s}_{t,l} \in \mathbb{C}^{K \times 1}$ and $\mathbf{n} \in \mathbb{C}^{N \times 1}$ denote the vectors with information signals and additive white Gaussian noise (AWGN), respectively. $\mathbf{s}_{t,l}$ is given by $\mathbf{s}_{t,l} = [\sqrt{P_1}s_{t,l,1}, \dots, \sqrt{P_K}s_{t,l,K}]^T$, where P_k represents the transmit power of drone k and $s_{t,l,k}$ refers to the t th signal in the l th subframe from drone k . When $t = 0$, $\mathbf{s}_{0,l}$ denotes the vector of pilot signal in the l th subframe. Since $s_{0,l,k} = 1$ for $k \in \{1, \dots, k\}$, $\mathbf{s}_{0,l} = [\sqrt{P_1}, \dots, \sqrt{P_K}]^T$. $\boldsymbol{\omega}(l) \triangleq$

$\text{diag}\{\eta_1 e^{j2\pi f_{D,1}l/f_s}, \dots, \eta_K e^{j2\pi f_{D,K}l/f_s}\}$ refers to a diagonal matrix with path loss and Doppler frequency, where f_s denotes the signal sampling frequency and η_k indicates the free space path loss with the definition $\eta_k = \frac{\lambda}{4\pi d_k}$, d_k represents the distance between drone k and the BS. \mathbf{A} represents the array manifold of the BS, which can be denoted by $\mathbf{A} = [\mathbf{a}(\theta_1), \dots, \mathbf{a}(\theta_K)]$, in which the steering vector $\mathbf{a}(\theta_k)$ can be expressed as

$$\mathbf{a}(\theta_k) = [a_1(\theta_k), \dots, a_N(\theta_k)]^T, \quad (2)$$

where $a_n(\theta_k) \triangleq e^{-j2\pi(n-1)d \sin \theta_k/\lambda}$, $n \in \{1, \dots, N\}$.

III. SIMULTANEOUS COMMUNICATION AND TRACKING

The frame structure shown in Fig. 1 is employed for the PASCAT system to track the drones and decode the transmitted symbols from the drones. In the l th subframe of frame v for $v \in \{1, \dots, V\}$, l pilots are utilised to estimate the location parameters, which are then employed for decoding the T symbols in that subframe. It is worth mentioning that both the localisation and decoding performance in the l th subframe can be enhanced compared to that of the $l-1$ th subframe as more pilots are employed. When $l = L$, the final estimation for the location parameters can be obtained and decoding of the T symbols in the last subframe of frame v can be completed. In frame $v+1$, the above procedure is repeated to estimate the location parameters and decode the symbols in the new frame. By using this method, disjoint tracking and decoding can be achieved.

A. ML-based Algorithm for Tracking

In this section, an ML-based algorithm is proposed for PTD to estimate the location parameters in each frame by using an increased number of pilots, where the locations and velocities of drones change once every frame cycle. In the l th subframe of frame v , the pilot signal vector can be given by

$$\mathbf{y}_1 = \left\{ \left\{ \mathbf{A}\boldsymbol{\omega}(1)\mathbf{s}_{0,1} \right\}^T, \dots, \left\{ \mathbf{A}\boldsymbol{\omega}(l)\mathbf{s}_{0,l} \right\}^T \right\}^T + \mathbf{n}_1, \quad (3)$$

where $\mathbf{y}_1 \in \mathbb{C}^{Nl \times 1}$ contains the first l pilot signals. \mathbf{y}_1 follows a multivariate Gaussian distribution and thus its PDF is shown as

$$f(\mathbf{y}_1|\boldsymbol{\psi}) = \frac{1}{\pi^{MNl} \det(\boldsymbol{\Gamma})} e^{-\frac{(\mathbf{y}_1 - \boldsymbol{\mu})^H (\mathbf{y}_1 - \boldsymbol{\mu})}{\boldsymbol{\Gamma}}}, \quad (4)$$

where $\boldsymbol{\psi} = [\boldsymbol{\theta}^T, \mathbf{d}^T, \mathbf{f}_D^T]^T$ represents a vector composed of the deterministic unknown location parameters, in which $\boldsymbol{\theta} = [\theta_1, \dots, \theta_K]$, $\mathbf{d} = [d_1, \dots, d_K]$ and $\mathbf{f}_D = [f_{D,1}, \dots, f_{D,K}]$. $\boldsymbol{\mu}$ and $\boldsymbol{\Gamma}$ indicates the mean vector and covariance matrix, respectively. $\boldsymbol{\mu} = \left\{ \left\{ \mathbf{A}\boldsymbol{\omega}(1)\mathbf{s}_{0,1} \right\}^T, \dots, \left\{ \mathbf{A}\boldsymbol{\omega}(l)\mathbf{s}_{0,l} \right\}^T \right\}^T$ and $\boldsymbol{\Gamma} = \sigma^2 \mathbf{I}$, in which σ^2 and \mathbf{I} refer to the variance of AWGN and the identity matrix.

By using the PDF of the received signal vector in (4), the maximum likelihood estimator (MLE) can be given by

$$\begin{aligned} \hat{\boldsymbol{\psi}} &= \arg \max_{\boldsymbol{\psi}} \ln f(\mathbf{y}_1|\boldsymbol{\psi}) \\ &= \arg \min_{\boldsymbol{\psi}} \|\mathbf{y}_1 - \boldsymbol{\mu}\|_2^2. \end{aligned} \quad (5)$$

where the output of MLE in (5) provides the estimation of location parameters in the l th subframe of frame v , which can be denoted by $\hat{\boldsymbol{\psi}}_l$. With the increase of pilots, the localisation performance can be improved, thus the estimation results in

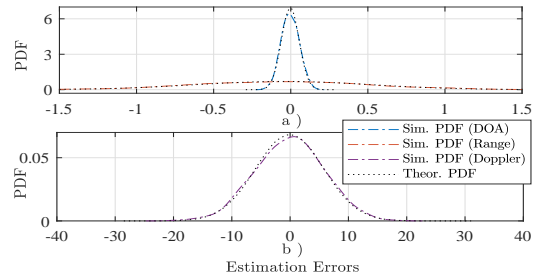


Fig. 2. PDF of the estimation errors for location parameters.

$l+1$ th subframe will be more accurate than that of l th subframe. When $l = L$, the final estimation for location parameters can be obtained. Furthermore, the tracking of drones can be achieved by repeating the above-mentioned process when the positions and velocities of drones change every frame interval.

In addition to tracking drones by using pilot signals directly, we can also employ the initial estimates of location parameters obtained in multiple subframes, each of which is estimated by using MLE in (5) with a single pilot signal in each subframe. It is worth mentioning that the derived MLE in (5) is general for a received signal vector with multiple pilot signals, thus it can be directly used in ETD, which employs multiple single-pilot signals to provide the initial estimates, as shown in Fig. 1. Given that the estimated location parameters with MLE follow Gaussian distributions with means equal to their actual values, calculating the average of the initial estimates of location parameters is nearly equivalent to using pilot signals directly for tracking, and thus ETD can achieve performance close to that of PTD.

B. Data Decoding

In the communication stage, the estimated location parameters obtained in Sec. III-A are employed to infer the channel responses, which are then fed into an MRC to preprocess the received signal to improve the signal quality. In the l th subframe, the received signal $\mathbf{y}_{t,l}$ is multiplied with the estimated channel response matrix $\hat{\mathbf{H}}$ as

$$\begin{aligned} \mathbf{x}_{t,l} &= \hat{\mathbf{H}}^H \mathbf{y}_{t,l} \\ &= [\hat{\mathbf{A}}\hat{\boldsymbol{\omega}}(l)]^H \mathbf{A}\boldsymbol{\omega}(l)\mathbf{s}_{t,l} + [\hat{\mathbf{A}}\hat{\boldsymbol{\omega}}(l)]^H \mathbf{n}, \end{aligned} \quad (6)$$

where $\mathbf{x}_{t,l} \in \mathbb{C}^{K \times 1}$. $\hat{\mathbf{A}}$ and $\hat{\boldsymbol{\omega}}(l)$ indicate the vectors consisting of the estimated location parameters in Sec. III-A. $\hat{\mathbf{A}}$ and $\hat{\boldsymbol{\omega}}(l)$ are written as $\hat{\mathbf{A}} = [\mathbf{a}(\hat{\theta}_1), \dots, \mathbf{a}(\hat{\theta}_K)]$ and $\hat{\boldsymbol{\omega}}(l) = \text{diag}\{\eta_1(\hat{d}_1)e^{j2\pi\hat{f}_{D,1}l/f_s}, \dots, \eta_K(\hat{d}_K)e^{j2\pi\hat{f}_{D,K}l/f_s}\}$, respectively. $\hat{\theta}_k$, \hat{d}_k and $\hat{f}_{D,k}$ for $k \in \{1, \dots, K\}$ can be written as $\hat{\theta}_k = \theta_k + \Delta\theta_k$, $\hat{d}_k = d_k + \Delta d_k$ and $\hat{f}_{D,k} = f_{D,k} + \Delta f_{D,k}$, in which $\Delta\theta_k$, Δd_k and $\Delta f_{D,k}$ denote the estimation errors for location parameters. It is found that the PDFs of the estimation errors follow the independent Gaussian distribution, as shown in Fig. 2. In Fig. 2, a BS composed of $N = 8$ antennas is employed to estimate the location of a drone, which is located at $(\theta, f_D, d) = [(40^\circ, 4000 \text{ Hz}, 80 \text{ m})]$, in frame v with $L = 50$ pilots. However, due to the presence of the noise, there are some estimation errors in estimating their location. By collecting samples of the estimation errors from 1000 tests at SNR = 12 dB, their PDFs are plotted in Fig. 2. Afterwards, by

calculating the mean and variance of the samples and comparing the PDF of the estimation errors to the theoretical Gaussian PDF with the same mean and variance as those of the estimation errors, it can be found that the estimation errors follow the Gaussian distribution with zero mean. This can be attributed to the fact that according to [28, Theorem 7.1], if the log-likelihood function of MLE is differentiable and the Fisher information is non-zero, the estimation errors of MLE follow the Gaussian distribution with zero mean and a variance that equals the inverse of Fisher information.

The k th element of $\mathbf{x}_{t,l}$ in (6) can be given by

$$x_{t,l,k} = \sqrt{P_K} \hat{\mathbf{h}}_k^H \mathbf{h}_k s_{t,l,k} + \sum_{\tilde{p}=1, \tilde{p} \neq k}^K \sqrt{P_{\tilde{p}}} \hat{\mathbf{h}}_k^H \mathbf{h}_{\tilde{p}} s_{t,l,\tilde{p}} + \hat{\mathbf{h}}_k^H \mathbf{n}, \quad (7)$$

where $\hat{\mathbf{h}}_k$ indicates the estimated channel response of drone k , which is composed of estimated location parameters as $\hat{\mathbf{h}}_k = \eta_k(\hat{d}_k) \mathbf{a}(\hat{\theta}_k) e^{j2\pi(f_{D,k})/f_s}$, \mathbf{h}_k and $\mathbf{h}_{\tilde{p}}$ refer to the actual channel response of drone k and drone \tilde{p} , which can be represented by using a general expression as $\mathbf{h}_\zeta = \eta_\zeta \mathbf{a}(\theta_\zeta) e^{j2\pi f_{D,\zeta}/f_s}$, where $\zeta \in \{k, \tilde{p}\}$. Since the estimated location parameters contain estimation errors, $\hat{\mathbf{h}}_k$ can also be written as

$$\hat{\mathbf{h}}_k = \eta_k(d_k + \Delta d_k) \mathbf{a}(\theta_k + \Delta \theta_k) e^{j2\pi(f_{D,k} + \Delta f_{D,k})/f_s}, \quad (8)$$

where since Δd_k , $\Delta \theta_k$ and $\Delta f_{D,k}$ are random, $\hat{\mathbf{h}}_k$ is random.

Thereafter, we provide the performance analysis in Sec. IV to evaluate the tracking and data decoding performance of DTDD.

IV. PERFORMANCE ANALYSIS FOR DTDD

A. Conditional SER for MPSK

In order to obtain the average SER for M -ary Phase Shift Keying (MPSK), the conditional SER given the estimation errors of location parameters $\Delta \boldsymbol{\psi} = [\Delta \theta, \Delta f_D]^T$, which can be calculated by using $\Delta \boldsymbol{\psi} = \hat{\boldsymbol{\psi}} - \boldsymbol{\psi}$, should be derived first. This is due to the fact that it is difficult to derive average SER directly as the PDF of the received signal $x_{t,l,k}$ is unknown and the derivation of this PDF is not straightforward by noting that each item of the received signal in (7) is highly correlated since they contain the same random vector $\hat{\mathbf{h}}_k^H$. To begin, by considering all possible phase-shifted signal combinations transmitted by different drones, the conditional SER can be calculated by using

$$P_e | \Delta \boldsymbol{\psi} = \sum_{m_1, \dots, m_K \in S_1} \frac{P_e | \{\Delta \boldsymbol{\psi}, \beta\}}{M^K}, \quad (9)$$

where $\beta = \{s_{t,l,1} = s_{t,l,1}(m_1), \dots, s_{t,l,K} = s_{t,l,K}(m_K)\}$ represents a case of phase-shifted signal combination, in which, for instance, drone 1 and drone K are transmitting $s_{t,l,1}(m_1)$ and $s_{t,l,K}(m_K)$, respectively. $s_{t,l,1}, \dots, s_{t,l,K}$ can be expressed by using a general expression as $s_{t,l,k}$, which denotes the t th signal vector with all possible phases transmitted by drone k in the l th subframe and $s_{t,l,k}$ is written as $s_{t,l,k} = [1, \dots, e^{\frac{j2\pi(M-1)}{M}}]$. It is worth mentioning that each phase of the transmitted signal is assumed to be equally likely in MPSK. $S_1 = \{1, 2, \dots, M\}$, in which M indicates the number of phases in modulating the signals.

By noting that the only random parameter in $x_{t,l,k}$ given $\Delta \boldsymbol{\psi}$

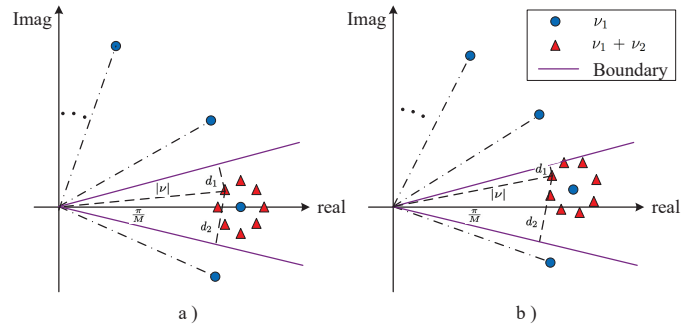


Fig. 3. Illustrations of union bound method for MPSK a) with perfect localisation b) with imperfect localisation for two drones.

is noise \mathbf{n} , the PDF of $x_{t,l,k}$ conditioned on $\Delta \boldsymbol{\psi}$ can be given by

$$f(x_{t,l,k} | \Delta \boldsymbol{\psi}) = \frac{1}{\Gamma_x} e^{-\frac{(x_{t,l,k} - \mu_x)^* (x_{t,l,k} - \mu_x)}{\Gamma_x}}, \quad (10)$$

where μ_x and Γ_x refers to the mean and variance of $x_{t,l,k}$. μ_x

can be written as $\mu_x = \sqrt{P_K} \hat{\mathbf{h}}_k^H \mathbf{h}_k s_{t,l,k} + \sum_{\tilde{p}=1, \tilde{p} \neq k}^K \sqrt{P_{\tilde{p}}} \hat{\mathbf{h}}_k^H \mathbf{h}_{\tilde{p}} s_{t,l,\tilde{p}}$.

Γ_x can be calculated by using

$$\begin{aligned} \Gamma_x &= \mathbb{E}[(x_{t,l,k} - \mu_x)^* (x_{t,l,k} - \mu_x)] \\ &= \sum_{i=1}^N \sum_{j=1}^N \hat{h}_{k,i} \hat{h}_{k,j}^* \mathbb{E}[n_i^* n_j], \end{aligned} \quad (11)$$

where $\hat{h}_{k,i}$ and $\hat{h}_{k,j}$ indicate the i th and j th element of $\hat{\mathbf{h}}_k$, while n_i and n_j refer to the i th and j th element of \mathbf{n} . By performing some simple algebraic manipulations and noting that $\hat{h}_{k,i} \hat{h}_{k,j}^* = \eta_k^2(\hat{d}_k)$ for $i = j$, Γ_x can be simplified to $\Gamma_x = N \eta_k^2(\hat{d}_k) \sigma^2$.

Based on the conditional PDF in (10), $P_e | \{\Delta \boldsymbol{\psi}, \beta\}$ can be derived by using the union bound method, which is illustrated in Fig. 3 by using an example of two drones. It is worth mentioning that even if Fig. 3 uses an example of two drones, our derivation for the conditional SER is general for multiple drones. In Fig. 3, the blue circles and red triangles denote the constellation points considering drone 1 and the constellation points considering drone 1 and drone 2, in which the signal transmitted from drone 2 is considered as the interference signal when we are decoding the symbols from drone 1. d_1 and d_2 refer to the distance from the constellation point to the boundary lines without the influence of the noise term. $|\nu|$ indicates the distance between the constellation point and the origin of the coordinate axis.

In Fig. 3, the union bound methods with the perfect localisation case and the imperfect localisation case for deriving the conditional MPSK are compared. When the perfect localisation case is considered, the only interference affecting the data decoding process is the noise \mathbf{n} . However, both \mathbf{n} and the location errors can affect the data decoding process when the imperfect localisation case is considered. Interestingly, it can be found that the constellation points are rotated in the imperfect localisation case compared to those of the perfect localisation case due to the localisation errors. In addition, the distance from the constellation points to the origin of the coordinate axis is also affected. In order to derive the conditioned MPSK, the

probability that the phase of the received signal lies outside the boundary lines is required, which can be obtained by calculating the probability that the distance from the received signal to the two boundary lines is respectively greater than d_1 and d_2 under the influence of the noise \mathbf{n} . Since $x_{t,l,k}$ given $\Delta\psi$ follow the Gaussian distribution, $P_e|\{\Delta\psi, \beta\}$ can be evaluated as

$$P_e|\{\Delta\psi, \beta\} = \frac{1}{\sqrt{\pi\Gamma_x}} \int_{d_1}^{\infty} e^{-\frac{z^2}{\Gamma_x}} dz + \frac{1}{\sqrt{\pi\Gamma_x}} \int_{d_2}^{\infty} e^{-\frac{z^2}{\Gamma_x}} dz, \quad (29)$$

where d_1 and d_2 can be respectively given by

$$d_1 = \sin\left(\frac{\pi}{M} - \arg(\nu)\right) |\nu| \\ = \left\{ \sin\frac{\pi}{M} \cos(\arg(\nu)) - \cos\frac{\pi}{M} \sin(\arg(\nu)) \right\} |\nu|, \quad (30a)$$

$$d_2 = \sin\left(\arg(\nu) + \frac{\pi}{M}\right) |\nu| \\ = \left\{ \sin\frac{\pi}{M} \cos(\arg(\nu)) + \cos\frac{\pi}{M} \sin(\arg(\nu)) \right\} |\nu|, \quad (30b)$$

where $\nu = \sqrt{P_k} \hat{\mathbf{h}}_k^H \mathbf{h}_k \mathbf{s}_{t,l,k}(m_k) + \sum_{\bar{p}=1, \bar{p} \neq k}^K \sqrt{P_{\bar{p}}} \hat{\mathbf{h}}_{\bar{k}}^H \mathbf{h}_{\bar{p}} \mathbf{s}_{t,l,\bar{p}}(m_{\bar{p}})$, in which $m_k, m_{\bar{p}} \in \{m_1, \dots, m_K\}$. To facilitate the subsequent analysis, we denote ν as $\nu = \sum_{p=1}^K \sqrt{P_p} \hat{\mathbf{h}}_k^H \mathbf{h}_p \mathbf{s}_{t,l,p}(m_p)$, in which $p \in \{1, \dots, K\}$.

By substituting the value of $\hat{\mathbf{h}}_k^H, \mathbf{h}_p, \mathbf{s}_{t,l,p}(m_p)$ into ν , ν can be written as

$$\nu = \sum_{p=1}^K \sum_{i=1}^N \eta_k(\hat{d}_k) \eta_p \sqrt{P_p} e^{j2\pi\left\{(i-1)d\Theta_p + \frac{m_p-1}{M} + \frac{f_{D,p} - f_{D,k} - \Delta f_{D,k}}{f_s}\right\}}, \quad (13)$$

where $\Theta_p = [\sin(\theta_k + \Delta\theta_k) - \sin\theta_p]/\lambda$. By using the small angle approximation (i.e., $\sin(\theta_k + \Delta\theta_k) = \sin\theta_k \cos\Delta\theta_k + \sin\Delta\theta_k \cos\theta_k \simeq \sin\theta_k + \Delta\theta_k \cos\theta_k$), Θ_p can be approximated as $\Theta_p \simeq [\sin\theta_k - \sin\theta_p + \Delta\theta_k \cos\theta_k]/\lambda$. It is worth mentioning that the small-angle approximation employed in this paper is very accurate since $\Delta\theta_k$ is small and distributes around zero with a variance that decreases considerably with the increase of SNR.

By replacing the integrals in (9) with Q functions, substituting $\Gamma_x = N\eta_k^2(\hat{d}_k)\sigma^2$ into (9) and then performing some algebraic

manipulations, $P_e|\{\Delta\psi, \beta\}$ in (9) can also be given by

$$P_e|\{\Delta\psi, \beta\} = Q_1 + Q_2, \quad (14)$$

where $Q_1 = Q\left(\frac{\sqrt{2}d_1}{\sqrt{N\eta_k^2(\hat{d}_k)\sigma^2}}\right)$ and $Q_2 = Q\left(\frac{\sqrt{2}d_2}{\sqrt{N\eta_k^2(\hat{d}_k)\sigma^2}}\right)$. By substituting the result of $P_e|\{\Delta\psi, \beta\}$ into (9), the conditioned SER for MPSK can be obtained.

B. Average SER for MPSK

Based on the conditional SER derived in Sec. IV-A, the average SER for MPSK can be calculated by using

$$P_e = \sum_{m_1, \dots, m_K \in S_1} \frac{\mathbb{E}[P_e|\{\Delta\psi, \beta\}]}{M^K}. \quad (15)$$

By substituting the derivation result of $P_e|\{\Delta\psi, \beta\}$ in (14) into (15), $P_e = \sum_{m_1, \dots, m_K \in S_1} \frac{\mathbb{E}[Q_1] + \mathbb{E}[Q_2]}{M^K}$ can be obtained. $\mathbb{E}[Q_{\ell_1}]$ for $\ell_1 \in \{1, 2\}$ can be calculated by using

$$\mathbb{E}[Q_{\ell_1}] = \mathbb{E}\left[Q\left(\frac{\sqrt{2}(\sin\frac{\pi}{M} \cos(\arg(\nu)) + (-1)^{\ell_1} \cos\frac{\pi}{M} \sin(\arg(\nu)) |\nu|)}{\sqrt{N\eta_k^2(\hat{d}_k)\sigma^2}}\right)\right], \quad (16)$$

where $\arg(\nu)$ can be given by

$$\arg(\nu) = \begin{cases} \arctan\left(\frac{\nu_y}{\nu_x}\right), & \text{if } \nu_x > 0 \\ \arctan\left(\frac{\nu_y}{\nu_x}\right) + \pi, & \text{if } \nu_x < 0 \text{ and } \nu_y \geq 0 \\ \arctan\left(\frac{\nu_y}{\nu_x}\right) - \pi, & \text{if } \nu_x < 0 \text{ and } \nu_y < 0 \\ \frac{\pi}{2}, & \text{if } \nu_x = 0 \text{ and } \nu_y > 0 \\ -\frac{\pi}{2}, & \text{if } \nu_x = 0 \text{ and } \nu_y < 0 \\ \text{undefined}, & \text{if } \nu_x = 0 \text{ and } \nu_y = 0 \end{cases} \quad (17)$$

where ν_x and ν_y represent the real and image part of ν .

Then by using $\cos(\arctan(x)) = \frac{1}{\sqrt{1+x^2}}$ and $\sin(\arctan(x)) = \frac{x}{\sqrt{1+x^2}}$, where x indicates the input of $\arctan(\cdot)$, and performing some algebraic operations, the simplified expression of $\mathbb{E}[Q_{\ell_1}]$ can be obtained, which are

$$\prod_{g_1=1}^{G_1} \prod_{g_2=1}^{G_2} \cos\theta_{g_1} \sin\theta_{g_2} = \begin{cases} \sum_{e_1, \dots, e_{G_1+G_2} \in S_1} \frac{(-1)^{\frac{G_2}{2}} \cos\left(\sum_{g=1}^{G_1+G_2} e_g \theta_g\right) \prod_{g=1}^{G_2} e_g}{2^{G_1+G_2}}, & \text{if } G_2 \text{ is even} \\ \sum_{e_1, \dots, e_{G_1+G_2} \in S_1} \frac{(-1)^{\frac{G_2-1}{2}} \sin\left(\sum_{g=1}^{G_1} e_g \theta_g + e_{G_1+1} [\theta_{G_1+1} + \sum_{g=G_1+2}^{G_1+G_2} e_g \theta_g]\right) \prod_{g=1}^{G_2} e_g}{2^{G_1+G_2}}, & \text{if } G_2 \text{ is odd} \end{cases} \quad (28)$$

represented by using a general expression as

$$\mathbb{E}[Q_{\ell_1}] = \begin{cases} \mathbb{E} \left[Q \left(\frac{\sqrt{2}\tilde{\nu}}{\sqrt{N\eta_k(\hat{d}_k)\sigma^2}} \right) \right], & \text{if } \nu_x \neq 0 \\ \mathbb{E} \left[Q \left(\frac{(-1)^{\ell_1}\sqrt{2}\cos\frac{\pi}{M}\nu_y}{\sqrt{N\eta_k(\hat{d}_k)\sigma^2}} \right) \right], & \text{if } \nu_x = 0 \text{ and } \nu_y \neq 0 \\ \text{undefined,} & \text{if } \nu_x = 0 \text{ and } \nu_y = 0 \end{cases} \quad (18)$$

where $\tilde{\nu} = \sin\frac{\pi}{M}\nu_x + (-1)^{\ell_1}\cos\frac{\pi}{M}\nu_y$.

In order to simplify the notation, $\mathbb{E} \left[Q \left(\frac{\sqrt{2}\tilde{\nu}}{\sqrt{N\eta_k(\hat{d}_k)\sigma^2}} \right) \right]$ and $\mathbb{E} \left[Q \left(\frac{(-1)^{\ell_1}\sqrt{2}\cos\frac{\pi}{M}\nu_y}{\sqrt{N\eta_k(\hat{d}_k)\sigma^2}} \right) \right]$ can be denoted by using \mathbb{E}_1 and \mathbb{E}_2 , respectively. To simplify \mathbb{E}_1 and \mathbb{E}_2 , $\eta_k(\hat{d}_k)$ can be extracted from $\tilde{\nu}$ and ν_y as $\tilde{\nu} = \eta_k(\hat{d}_k)\tilde{\nu}_1$ and $\nu_y = \eta_k(\hat{d}_k)\nu_{y1}$, in which

$$\tilde{\nu}_1 = \sin\frac{\pi}{M}\nu_{x1} + (-1)^{\ell_1}\cos\frac{\pi}{M}\nu_{y1}, \quad (19)$$

where ν_{x1} and ν_{y1} can be calculated by using $\nu_{x1} = \frac{\nu_x}{\eta_k(\hat{d}_k)}$ and $\nu_{y1} = \frac{\nu_y}{\eta_k(\hat{d}_k)}$, respectively. By using this simplification method, \mathbb{E}_1 and \mathbb{E}_2 can be simplified as $\mathbb{E} \left[Q \left(\frac{\sqrt{2}\tilde{\nu}_1}{\sqrt{N\sigma^2}} \right) \right]$ and $\mathbb{E} \left[Q \left(\frac{(-1)^{\ell_1}\sqrt{2}\cos\frac{\pi}{M}\nu_{y1}}{\sqrt{N\sigma^2}} \right) \right]$. It can be found that $\eta_k(\hat{d}_k)$ is cancelled out in \mathbb{E}_1 and \mathbb{E}_2 . As a consequence, we can conclude that the estimation errors for range have no effect on the average SER for MPSK using MRC.

Based on the above conclusion, \mathbb{E}_1 and \mathbb{E}_2 can be respectively evaluated as

$$\mathbb{E}_1 = \int_{\Delta f_{D,\min}}^{\Delta f_{D,\max}} \int_{-\pi}^{\pi} Q \left(\frac{\sqrt{2}\tilde{\nu}}{\sqrt{N\sigma^2}} \right) f(\Delta\theta_k) f(\Delta f_{D,k}) d\Delta\theta_k d\Delta f_{D,k}, \quad (19a)$$

$$\mathbb{E}_2 = \int_{\Delta f_{D,\min}}^{\Delta f_{D,\max}} \int_{-\pi}^{\pi} Q \left(\frac{\sqrt{2}C_1\nu_y}{\sqrt{N\sigma^2}} \right) f(\Delta\theta_k) f(\Delta f_{D,k}) d\Delta\theta_k d\Delta f_{D,k}, \quad (19b)$$

where $C_1 = (-1)^{\ell_1}\cos\frac{\pi}{M}$, $f(\Delta\theta_k)$ and $f(\Delta f_{D,k})$ denote the PDF of $\Delta\theta_k$ and $\Delta f_{D,k}$, respectively, which can be expressed by using a general expression shown as

$$f(\Delta\psi_k) = \frac{1}{\sqrt{2\pi}\sigma_\psi} e^{-\frac{1}{2}\left(\frac{\Delta\psi_k}{\sigma_\psi}\right)^2}, \quad (20)$$

where σ_ψ indicates the standard derivation of $\Delta\psi_k$.

Due to the fact that the Q functions in \mathbb{E}_1 and \mathbb{E}_2 are com-

posed of the sum of trigonometric functions, which contains random parameters following Gaussian distributions, there is no closed-form expression for \mathbb{E}_1 and \mathbb{E}_2 . As a consequence, the L th Taylor polynomial of the Q function is invoked to approximate $Q(x)$ in \mathbb{E}_1 and \mathbb{E}_2 , where $Q(x)$ indicates the Q functions and x denotes the input. To improve the approximation performance, the approximation of $Q(x)$ for x at the point x_0 is employed, in which x_0 the perfect case of x when there is no localisation errors (i.e., $\Delta\theta_k = 0$, $\Delta f_{D,k} = 0$). It is worth mentioning that this perfect estimation for location parameters can be obtained when SNR is very large. In addition, since $\Delta\theta_k$ and $\Delta f_{D,k}$ are small, this kind of Taylor approximation is very accurate even if L is small. Then the Taylor approximation of $Q(x)$ at x_0 can be denoted by

$$Q(x) \simeq \sum_{l=0}^L \frac{Q^{(l)}(x_0)(x-x_0)^l}{l!}, \quad (21)$$

where $Q^{(l)}(x_0)$ indicates the l th derivative of the Q function evaluated at x_0 and $Q^{(0)}(x_0) = Q(x_0)$. While for $l > 0$, $Q^{(l)}(x_0)$ can be expressed as

$$Q^{(l)}(x_0) = -\frac{1}{(\sqrt{2})^l\sqrt{\pi}} e^{-\frac{x_0^2}{2}} (-1)^{l+1} H_{l-1}\left(\frac{x_0}{\sqrt{2}}\right), \quad (22)$$

where $H_{l-1}\left(\frac{x_0}{\sqrt{2}}\right)$ denotes the $l-1$ th Hermite polynomial at $\frac{x_0}{\sqrt{2}}$. By using the approximation method, \mathbb{E}_1 and \mathbb{E}_2 can be approximated as

$$\mathbb{E}_{\ell_1} \simeq \sum_{l=0}^L \frac{(\sqrt{2})^l Q^{(l)}(x_{\ell_1,0})(C_1^l)^{\ell_1-1} \mathbb{E}_{\ell_1+2}}{(\sqrt{N\sigma^2})^l l!}, \quad (23)$$

where $x_{\ell_1,0} = \frac{\sqrt{2}\tilde{\nu}_{1,0}}{\sqrt{N\sigma^2}}$ if $\ell_1 = 1$ and $x_{\ell_1,0} = \frac{\sqrt{2}C_1\nu_{y1,0}}{\sqrt{N\sigma^2}}$ if $\ell_1 = 2$, in which $\tilde{\nu}_{1,0}$ and $\nu_{y1,0}$ indicate the perfect case for $\tilde{\nu}_1$ and ν_{y1} when there is no localisation errors. In addition, $\mathbb{E}_3 = \mathbb{E}[(\tilde{\nu}_1 - \tilde{\nu}_{1,0})^l]$ and $\mathbb{E}_4 = \mathbb{E}[(\nu_{y1} - \nu_{y1,0})^l]$, respectively.

To evaluate \mathbb{E}_3 and \mathbb{E}_4 , the binomial theorem needs to be used to expand the polynomials in \mathbb{E}_3 and \mathbb{E}_4 . Afterwards, \mathbb{E}_3 and \mathbb{E}_4 can be written as

$$\mathbb{E}_{\ell_1+2} = \sum_{q_1=0}^l \binom{l}{q_1} \mathbb{E}_{\ell_1+4} C_{\ell_1+2}^{l-q_1}, \quad (24)$$

where \mathbb{E}_{ℓ_1+4} can be given by $\mathbb{E}_5 = \mathbb{E}[\tilde{\nu}^{q_1}]$ and $\mathbb{E}_6 = \mathbb{E}[\nu_y^{q_1}]$,

$$\mathbb{E}_8 = \begin{cases} \sum_{e_1, \dots, e_{q_1} \in S_1} \frac{(-1)^{\frac{q_1}{2}} \mathbb{E}[\cos(C_2 C_3 \Delta\theta_k + 2\pi C_4 + 2\pi C_5 \Delta f_{D,k})] \prod_{g=1}^{q_1} e_g}{2^{q_1}}, & \text{if } q_1 \text{ is even} \\ \sum_{e_1, \dots, e_{q_1} \in S_1} \frac{(-1)^{\frac{q_1-1}{2}} \mathbb{E}[\sin(C_2 C_3 \Delta\theta_k + 2\pi C_4 + 2\pi C_5 \Delta f_{D,k})] \prod_{g=1}^{q_1} e_g}{2^{q_1}}, & \text{if } q_1 \text{ is odd} \end{cases} \quad (30)$$

$C_3 = -\tilde{\nu}_0$ and $C_4 = -\nu_{y,0}$. By substituting $\tilde{\nu} = \sin \frac{\pi}{M} \nu_x + (-1)^{\ell_1} \cos \frac{\pi}{M} \nu_y$ into \mathbb{E}_5 , \mathbb{E}_5 can also be represented as

$$\mathbb{E}_5 = \mathbb{E} \left[\sin \frac{\pi}{M} \nu_x + (-1)^{\ell_1} \cos \frac{\pi}{M} \nu_y \right]^{q_1}. \quad (25)$$

Afterwards, by applying the binomial theorem to \mathbb{E}_5 , \mathbb{E}_5 becomes

$$\mathbb{E}_5 = \sum_{q_2=0}^{q_1} \binom{q_1}{q_2} \left(\sin \frac{\pi}{M} \right)^{q_2} \left((-1)^{\ell_1} \cos \frac{\pi}{M} \right)^{q_1-q_2} \mathbb{E}_7, \quad (26)$$

where $\mathbb{E}_7 = \mathbb{E}[\nu_x^{q_2} \nu_y^{q_1-q_2}]$. It is worth mentioning that ν_x and ν_y in \mathbb{E}_6 and \mathbb{E}_7 are the sum of the cosine functions and sine functions by observing the expression of ν in (13).

To calculate \mathbb{E}_6 and \mathbb{E}_7 , the product-to-sum identities of the trigonometric formulas are employed to transform the product of trigonometric functions into a single cosine function or a single sine function to simplify the subsequent analysis. The employed trigonometric formulas are shown as

$$\begin{aligned} \prod_{g=1}^G \cos \theta_g &= \frac{1}{2^G} \sum_{e_1, \dots, e_G \in S_1} \cos \left(\sum_{g=1}^G e_g \theta_g \right), \quad (27a) \\ \prod_{g=1}^G \sin \theta_g &= \begin{cases} \sum_{e_1, \dots, e_G \in S_1} \frac{(-1)^{\frac{G}{2}} \cos \left(\sum_{g=1}^G e_g \theta_g \right) \prod_{g=1}^G e_g}{2^G}, & \text{if } G \text{ is even} \\ \sum_{e_1, \dots, e_G \in S_1} \frac{(-1)^{\frac{G-1}{2}} \sin \left(\sum_{g=1}^G e_g \theta_g \right) \prod_{g=1}^G e_g}{2^G}, & \text{if } G \text{ is odd} \end{cases} \end{aligned} \quad (27b)$$

and (28) at the bottom of page 6, in which G , G_1 and G_2 indicate the upper limit of the products and $S_1 = \{-1, 1\}^G$. By using these above trigonometric formulas and then performing some algebraic operations to simplify the result, \mathbb{E}_6 and \mathbb{E}_7 can also be expressed by using a general expression as

$$\mathbb{E}_{\ell_1+5} = \sum_{p_1, \dots, p_{q_1} \in S_2} \sum_{i_1, \dots, i_{q_1} \in S_3} \prod_{g=1}^{q_1} \eta_{p_g} \sqrt{P_{p_g}} \mathbb{E}_{\ell_1+7}, \quad (29)$$

where $S_2 \in \{1, \dots, K\}$, $S_3 \in \{1, \dots, N\}$, and $\ell_1 \in \{1, 2\}$. \mathbb{E}_8 is shown in (30) at the bottom of page 7 where $C_2 =$

$2\pi d \cos \theta_k / \lambda$, $C_3 = \sum_{g=1}^{q_1} e_g (i_g - 1)$ and $C_5 = -\frac{1}{f_s} \sum_{g=1}^{q_1} e_g$. In addition, C_4 can be written as

$$C_4 = \sum_{g=1}^{q_1} e_g \left[\underbrace{(i_g - 1)(\sin \theta_k - \sin \theta_{p_g}) d / \lambda + \frac{m_{p_g} - 1}{M} + \frac{f_{D,p_g} - f_{D,k}}{f_s}}_{\Phi_g} \right], \quad (31)$$

where it is worth mentioning that the notation i_g is employed to differentiate i in different summation operations and the same applies for η_{p_g} , P_{p_g} , $\sin \theta_{p_g}$, m_{p_g} , f_{D,p_g} and e_g .

Similar to \mathbb{E}_8 , \mathbb{E}_9 is shown in (32) at the bottom of page 8, in which

$$C_6 = \sum_{g=1}^{q_2} e_g (i_g - 1) + e_{q_2+1} [(i_{q_2+1} - 1) + \sum_{g=q_2+2}^{q_1} e_g (i_g - 1)], \quad (34)$$

where the two summation notations indicate the first q_2 summations and the last $(q_1 - q_2 - 1)$ summations, respectively.

Similarly, C_7 is shown in (35) at the bottom of page (35), where the definition of Φ_g is shown in (30). C_8 can be represented as

$$C_8 = -\frac{1}{f_s} \left[\sum_{g=1}^{q_2} e_g + e_{q_2+1} \left(1 + \sum_{g=q_2+2}^{q_1} e_g \right) \right]. \quad (36)$$

To evaluate the double integrals in \mathbb{E}_{10} , \mathbb{E}_{11} and \mathbb{E}_{12} in (30) and (32), the inner integrals with respect to $\Delta \theta_k$ should be calculated first by taking $\Delta f_{D,k}$ as a constant. Afterwards, the results of the inner integrals will be integrated with respect to $\Delta f_{D,k}$. By substituting the expression of $f(\Delta \theta_k)$ shown in (20) into \mathbb{E}_{10} and then using Euler's formula, the inner integral in \mathbb{E}_{10} can be denoted by

$$\begin{aligned} I_{10} &= \frac{1}{\sqrt{2\pi}\sigma_\theta} \int_{-\pi}^{\pi} \cos(C_2 C_3 \Delta \theta_k + C_9) e^{-\frac{1}{2} \left(\frac{\Delta \theta_k}{\sigma_\theta} \right)^2} d\Delta \theta_k \\ &= \frac{1}{2\sqrt{2\pi}\sigma_\theta} (e^{jC_9} I_1 + e^{-jC_9} I_2), \end{aligned} \quad (37)$$

$$\mathbb{E}_9 = \begin{cases} \sum_{e_1, \dots, e_{q_1} \in S_1} \frac{(-1)^{\frac{q_1-q_2}{2}} \mathbb{E}[\cos(C_2 C_3 \Delta \theta_k + 2\pi C_4 + 2\pi C_5 \Delta f_{D,k})] \prod_{g=q_2+1}^{q_1} e_g}{2^{q_1}}, & \text{if } q_1 - q_2 \text{ is even} \\ \sum_{e_1, \dots, e_{q_1} \in S_1} \frac{(-1)^{\frac{q_1-q_2-1}{2}} \mathbb{E}[\sin(C_2 C_6 \Delta \theta_k + 2\pi C_7 + 2\pi C_8 \Delta f_{D,k})] \prod_{g=q_2+1}^{q_1} e_g}{2^{q_1}}, & \text{if } q_1 - q_2 \text{ is odd} \end{cases} \quad (32)$$

$$C_7 = \sum_{g=1}^{q_2} e_g \Phi_g + e_{q_2+1} \left\{ \sum_{g=q_2+2}^{q_1} e_g \Phi_g + (i_{q_2+1} - 1) d \lambda (\sin \theta_k - \sin \theta_{p_{q_2+1}}) + \frac{m_{p_{q_2+1}} - 1}{M} + \frac{f_{D,p_{q_2+1}} - f_{D,k}}{f_s} \right\}, \quad (35)$$

TABLE I
SIMULATION PARAMETERS

Param.	Value	Param.	Value	Param.	Value
θ_1	20°	d_1	80 m	$f_{D,1}$	2kHz
θ_2	40°	d_2	80 m	$f_{D,2}$	4kHz
v_1	3.4 m/s	v_2	8.4 m/s	K	2
T	100	f_s	100 kHz	λ	1.6 mm

and the inner integrals in \mathbb{E}_{11} and \mathbb{E}_{12} can be represented as

$$I_{11} = \frac{1}{\sqrt{2\pi}\sigma_\theta} \int_{-\pi}^{\pi} \sin(C_2 C_3 \Delta\theta_k + C_9) e^{-\frac{1}{2} \left(\frac{\Delta\theta_k}{\sigma_\theta}\right)^2} d\Delta\theta_k$$

$$= \frac{1}{j2\sqrt{2\pi}\sigma_\theta} (e^{jC_9} I_1 - e^{-jC_9} I_2) \quad (38)$$

$$I_{12} = \frac{1}{\sqrt{2\pi}\sigma_\theta} \int_{-\pi}^{\pi} \sin(C_2 C_6 \Delta\theta_k + C_{10}) e^{-\frac{1}{2} \left(\frac{\Delta\theta_k}{\sigma_\theta}\right)^2} d\Delta\theta_k$$

$$= \frac{1}{j2\sqrt{2\pi}\sigma_\theta} (e^{jC_{10}} I_3 - e^{-jC_{10}} I_4), \quad (39)$$

where $C_9 = 2\pi C_4 + 2\pi C_5 \Delta f_{D,k}$ and $C_{10} = 2\pi C_7 + 2\pi C_8 \Delta f_{D,k}$. I_1, I_2, I_3 and I_4 can be expressed by using a general expression as

$$I_5 = \int_{-\pi}^{\pi} e^{\pm j C_{11} \Delta\theta_k - \frac{1}{2\sigma_\theta^2} \Delta\theta_k^2} d\Delta\theta_k, \quad (40)$$

where $C_{11} \in \{C_2 C_3, C_2 C_6\}$. The complete derivation of I_5 can be found in Appendix A. By substituting the derived closed-form expression of I_5 , the results of I_1, I_2, I_3 and I_4 can be obtained, which are then substituted into (37) and (38) to obtain the closed-form expressions of I_{10}, I_{11} and I_{12} .

Thereafter, the result of I_{10}, I_{11} and I_{12} can be integrated with respect to $\Delta f_{D,k}$ to calculate \mathbb{E}_{10} as

$$\mathbb{E}_{10} = \int_{\Delta f_{D,\min}}^{\Delta f_{D,\max}} I_{10} e^{-\frac{1}{2} \left(\frac{\Delta f_{D,k}}{\sigma_{fD}}\right)^2} d\Delta f_{D,k}$$

$$= \frac{1}{4\pi\sigma_\theta\sigma_{fD}} (e^{j2\pi C_4} I_1 I_6 + e^{-j2\pi C_4} I_2 I_7), \quad (41)$$

and \mathbb{E}_{11} and \mathbb{E}_{12} can be written as

$$\mathbb{E}_{11} = \int_{\Delta f_{D,\min}}^{\Delta f_{D,\max}} I_{11} e^{-\frac{1}{2} \left(\frac{\Delta f_{D,k}}{\sigma_{fD}}\right)^2} d\Delta f_{D,k}$$

$$= \frac{1}{j4\pi\sigma_\theta\sigma_{fD}} (e^{j2\pi C_4} I_1 I_6 - e^{-j2\pi C_4} I_2 I_7), \quad (42a)$$

$$\mathbb{E}_{12} = \int_{\Delta f_{D,\min}}^{\Delta f_{D,\max}} I_{12} e^{-\frac{1}{2} \left(\frac{\Delta f_{D,k}}{\sigma_{fD}}\right)^2} d\Delta f_{D,k}$$

$$= \frac{1}{j4\pi\sigma_\theta\sigma_{fD}} (e^{j2\pi C_7} I_3 I_8 - e^{-j2\pi C_7} I_4 I_9), \quad (42b)$$

where I_1, I_2, I_3 and I_4 have been derived and thus they are constants in (41) and (42a). I_6, I_7, I_8 and I_9 can be expressed by using a general expression as

$$I_{13} = \int_{\Delta f_{D,\min}}^{\Delta f_{D,\max}} e^{\pm j C_{12} \Delta f_{D,k} - \frac{1}{2\sigma_{fD}^2} \Delta f_{D,k}^2} d\Delta f_{D,k}, \quad (43)$$

where $C_{12} \in \{2\pi C_5, 2\pi C_8\}$. The complete derivation of I_{13} can be found in Appendix A. By using the derived closed-form expression of I_{13}, I_6, I_7, I_8 and I_9 can be obtained, which are

then substituted into (41) and (42a) to obtain the closed-form expressions of $\mathbb{E}_{10}, \mathbb{E}_{11}$ and \mathbb{E}_{12} .

The derived $\mathbb{E}_{10}, \mathbb{E}_{11}$ and \mathbb{E}_{12} are substituted into (30) and (32) to obtain \mathbb{E}_8 and \mathbb{E}_9 , which are then substituted into (28) to obtain \mathbb{E}_6 and \mathbb{E}_7 . By using the result of $\mathbb{E}_7, \mathbb{E}_5$ can be calculated according to (26). Thereafter, \mathbb{E}_5 and \mathbb{E}_6 can be substituted into (24) to calculate \mathbb{E}_3 and \mathbb{E}_4 . Finally, \mathbb{E}_1 and \mathbb{E}_2 can be derived by substituting \mathbb{E}_3 and \mathbb{E}_4 into (36) and thus then $\mathbb{E} \left[Q \left(\frac{\sqrt{2}\nu}{\sqrt{N}\sigma^2} \right) \right]$ and $\mathbb{E} \left[Q \left(\frac{(-1)^{\ell_1} \sqrt{2} \cos \frac{\pi}{M} \nu_y}{\sqrt{N}\sigma^2} \right) \right]$ can be obtained. According to (18), $\mathbb{E}[Q_{\ell_1}]$ can be calculated by using $\mathbb{E} \left[Q \left(\frac{\sqrt{2}\nu}{\sqrt{N}\sigma^2} \right) \right]$ and $\mathbb{E} \left[Q \left(\frac{(-1)^{\ell_1} \sqrt{2} \cos \frac{\pi}{M} \nu_y}{\sqrt{N}\sigma^2} \right) \right]$, which can be substituted into $P_e = \sum_{m_1, \dots, m_K \in S_1} \frac{\mathbb{E}[Q_1] + \mathbb{E}[Q_2]}{M^K}$ to obtain P_e .

V. NUMERICAL RESULTS

This section presents the simulation results and analytical results to evaluate the performance of the PASCAT system, where root mean squared error (RMSE) and SER are adopted as the localisation performance metric and communication performance metric, respectively. The simulation parameters can be found in Table I, where Param. indicates parameter. In addition, the transmit power of the signals from drone 1 and drone 2 is considered to be the same, and thus $P_1 = P_2$. In each simulation point, 1000 Monte Carlo tests are conducted.

In Fig. 4, the trajectories of drone 1 and drone 2 are estimated by using the ML-based algorithm in Sec. III-A. In the simulation, the BS is composed of $N = 8$ antennas, $L = 50$ pilots and SNR = 12 dB are employed. In Fig. 4, Traj. and Esti. Traj. denote real trajectory and estimated trajectory, respectively. It can be found that the estimated trajectory and the real trajectory match perfectly for both drone 1 and drone 2. For instance, the estimated locations of drone 1 and drone 2 by using MLE are $(\theta, f_D, d) = [(44.704^\circ, 0.102 \text{ Hz}, 75.481 \text{ m}), (45.103^\circ, 0.203 \text{ Hz}, 24.955 \text{ m})]$ when the drones are located at $(\theta, f_D, d) = [(45.000^\circ, 0.000 \text{ Hz}, 75.000 \text{ m}), (45.000^\circ, 0.000 \text{ Hz}, 25.000 \text{ m})]$. This indicates the efficiency of the ML-based algorithm in tracking. Since the tracking in the PASCAT system is achieved by localising and collecting the positions of drones in each frame, without loss of generality, we employ the localisation accuracy at frame v as an example to reflect the overall tracking performance in the subsequent results.

In Fig. 5, the synergy relationship between the localisation part and the communication part of the PASCAT system is demonstrated. In the simulation, a BS composed of $N = 6$ antennas is employed to localise and serve drone 1 and drone 2, and $L = 5$ pilots are contained in each frame. In addition, three modulation types including QPSK, 8PSK and 16PSK considered and MRC is employed to preprocess the received signal. To obtain the curves in Fig. 5, SNR has been changed from 0 dB to 24 dB. As can be observed from the results, RMSE has a positive effect on SER since a smaller RMSE corresponds to a lower SER. It should be noted that the RMSE and SER in Fig. 5 represent the average values of the RMSEs and SERs for two drones. This conclusion applies to the curves generated by using the three modulation schemes. This phenomenon can be

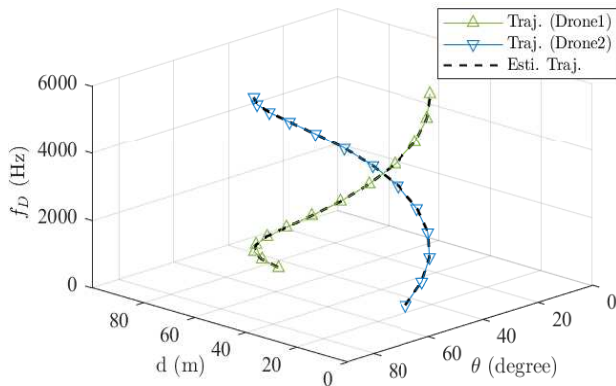


Fig. 4. The trajectory estimations of two drones.

attributed to the fact that the channel information is obtained by using the estimated location parameters in each frame. However, there are some estimation errors due to the presence of AWGN, which leads to erroneous channel estimation. As a consequence, an improved localisation accuracy results in a lower SER. The performance gap between the imperfect SER with the perfect case, which is obtained by combining the perfect estimation of channel information with the received signal by using the MRC technique and serves as a benchmark, is also shown in Fig. 5. In addition, analytical results and simulated results of SER match perfectly for all modulation types, where the $L = 6$ th Taylor approximation is employed to obtain the analytical result. For example, the gap between the analytical result and the simulated result is 6.6248×10^{-5} when the RMSE of DOA is 0.55 degrees and QPSK is employed.

In Fig. 6, both the communication and tracking performance of the PASACT system with the increase of pilot number is demonstrated. Without loss of generality, we employ the localisation for drone 1 and drone 2 in frame v as an example to indicate the tracking performance of the PASACT system. Since the localisation and data decoding of different subframes in frame v are based on a varying number of pilot signals, it is essential to investigate the impact of the number of pilots on them. In the simulation, we consider a BS consisting of $N = 6$ antennas and employ the ML-based tracking algorithm to obtain the location parameters and MRC to preprocess the received signal. In addition, 8PSK is used as the modulation method. As can be observed from Fig. 6, both the localisation and communication performance improve with the increase in the number of pilot signals. This indicates that the pilot number has a positive effect on both the localisation and communication functions of the proposed PASACT system. This phenomenon is due to the fact that the localisation accuracy or tracking accuracy is enhanced by using more pilots, which results in a more accurate acquisition of channel information and a better data decoding result. In addition, the analytical results obtained by using $L = 6$ th approximation orders and the simulation results match very well.

In Fig. 7, the performance of MRC is compared to that of the maximum likelihood detector (MLD) in different subframes in frame v . Notably, MLD is conducted by estimating DOA, range, Doppler frequency and symbol jointly, and thus it can provide the optimal results and is employed here as a benchmark. Since

different subframes are composed of varying numbers of pilot signals, the localisation and communication performance of the PASCAT system also differ accordingly. In Fig. 7, three subframes, which contain $l = 3$, $l = 5$ and $l = 30$ pilots, are considered. In addition, the BS is composed of $N = 5$ antennas, the total number of pilots in frame v is set to $L = 30$ and the modulation scheme is 8PSK. Due to the fact that the complexity of MLD increases exponentially with the number of estimation parameters, without loss of generality, we consider a single drone 1 in Fig. 7. Furthermore, to ensure a fair comparison, both MRC and MLD are based on l pilot signals and one symbol signal. The result shows that the gap between MRC and MLD reduces with the increase in the number of pilot signals, and MRC can achieve performance comparable to that of MLD. For instance, the gap between MRC and MLD is only 8.2×10^{-6} when $l = 30$ at SNR = 9 dB. Interestingly, this result demonstrates the efficiency of the PASCAT system as its performance improves with subframes and it can approach that of MLD when the number of pilots is large. The analytical result is also provided for MRC by using the 6th order Taylor approximation. The result indicates that the analytical and simulated results match very well.

In Fig. 8, the performance of the ML-based algorithm in Sec. III-A and MRC is compared with that of CRLB and MMSE, respectively. Notably, MMSE is employed here as a benchmark by assuming the estimation of location parameters is perfect and then using the perfectly estimated results to preprocess the received signal. In the simulation, $L = 5$ pilots are employed for tracking drone 1 and drone 2, and 8PSK is adopted as the modulation scheme. As can be observed from Fig. 8 that the performance of the ML-based algorithm approaches that of CRLB across the whole SNR range and even converges with it when SNR is high, which indicates the efficiency of the ML-based tracking algorithm. It can also be found from Fig. 8 that the performance gap between MRC and MMSE reduces with the increase in the number of antennas. This can be attributed to the fact that the estimation errors of location parameters in tracking decrease when more antennas are utilised in the BS. Furthermore, the analytical and simulated results for SER with MRC match perfectly during the entire SNR range, where the approximation order is $L = 6$.

In Fig. 9, the approximation error of the Taylor approximation method in Sec. IV-B is shown, where $L = 5$ pilots are employed to localise drone 1 and drone 2 at SNR = 3 dB and the modulation type is 8PSK. It is worth mentioning that the approximation error is obtained by computing the average of the gaps between the analytical and simulated results of SERs corresponding to the two targets by using MRC. In addition, three cases including $N = 5$, $N = 7$ and $N = 30$ are considered. The result shows that the approximation error reduces quickly with the increase of approximation order L and convergences when $L \geq 5$.

VI. CONCLUSION

This paper provided a SER analysis for the PASCAT system, in which we adopted multiple drones to actively send signals to a BS, which was responsible for tracking the drones in

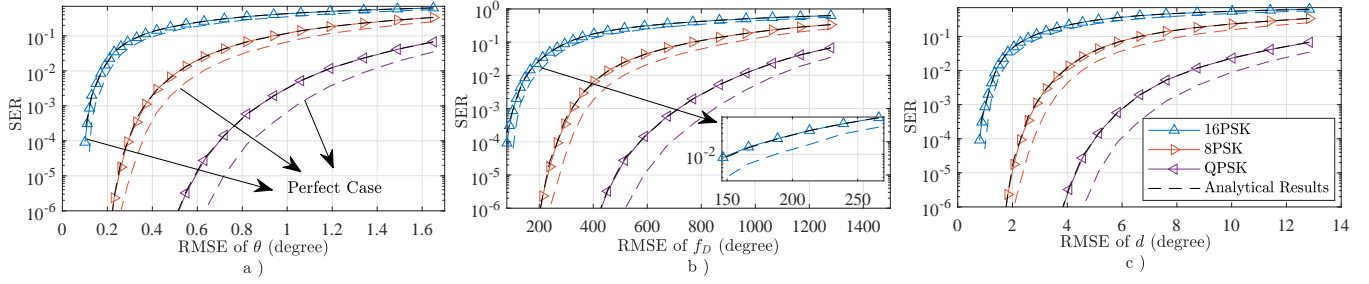


Fig. 5. The SERs with RMSEs of a) DOA θ , b) Doppler frequency f_D , c) Range d

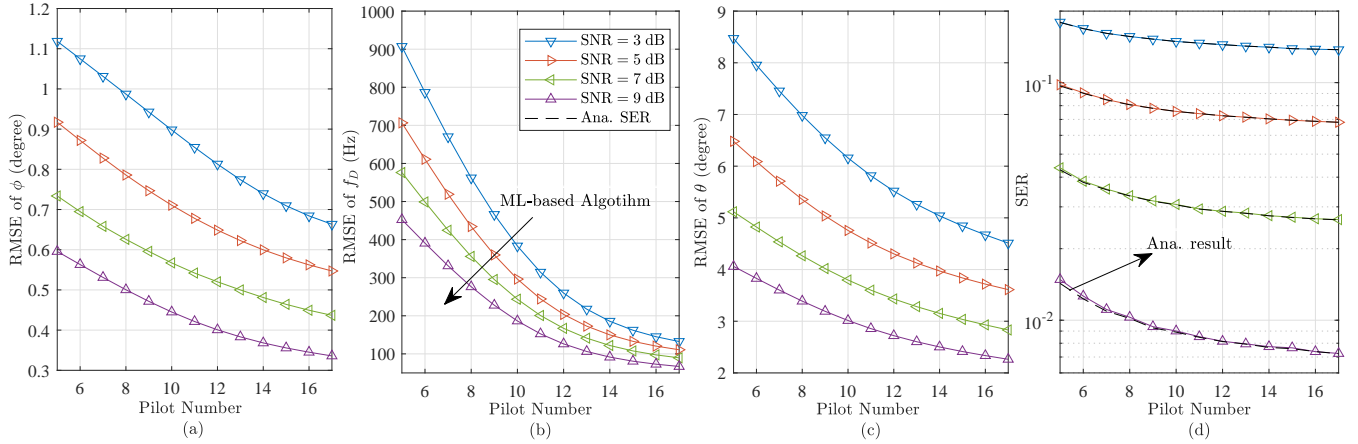


Fig. 6. The a) RMSE of DOA θ , b) RMSE of Doppler frequency f_D , c) RMSE of Range d , d) SER with the increase of the number of pilots

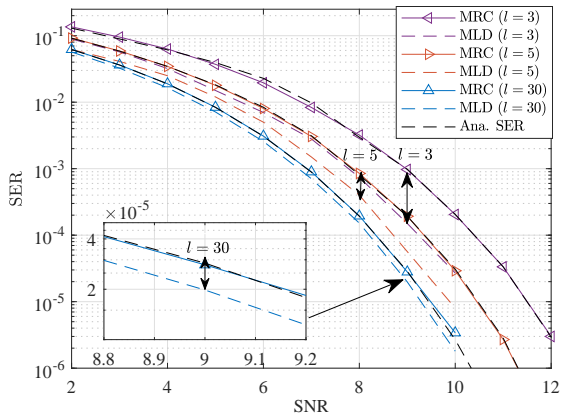


Fig. 7. The performance gap between MRC and MLD.

addition to decoding the symbols transmitted from these drones. To continuously determine the position of these drones, an ML-based tracking algorithm was proposed, which achieved performance comparable to CRLB. Afterwards, the estimated location parameters at a certain moment during the tracking process were employed to obtain CSI, which was then utilised to preprocess the received signal with MRC before data decoding. An approximation for the average SER was derived by using the Taylor approximation. Simulation results indicated that the approximation error converged when $L \geq 5$. In addition, the decoding performance with MRC in the PASCAT system was compared to that of MMSE and MLD. It was found that the decoding performance with MRC could approach that of the

latter two in some cases. In the end, the analytical and simulation results matched perfectly, which verified the accuracy of our analysis.

APPENDIX A THE COMPLETE DERIVATIONS OF I_5 AND I_{10}

To begin, I_5 and I_{13} can be given by using a general expression as

$$I_\psi = \int_{\Delta\psi_{\min}}^{\Delta\psi_{\max}} e^{\pm jC_{20}\Delta\psi_k - \frac{1}{2\sigma_\psi^2}\Delta\psi_k^2} d\Delta\psi_k, \quad (44)$$

where $C_{20} \in \{C_{16}, C_{17}\}$ and $\Delta\psi_k \in \{\Delta\theta_k, \Delta f_{D,k}\}$. $\Delta\psi_{\min}$ and $\Delta\psi_{\max}$ represents the minimum and maximum values of $\Delta\psi_k$, and σ_ψ indicates the variance of $\Delta\psi_k$.

By performing some algebraic operations, I_ψ can be written as

$$I_\psi = \int_{\Delta\psi_{\min}}^{\Delta\psi_{\max}} e^{-\left(\sqrt{\frac{1}{2\sigma_\psi^2}}\Delta\psi_k \mp \frac{jC_{20}}{2\sqrt{\frac{1}{2\sigma_\psi^2}}}\right)^2 - \frac{C_{20}^2\sigma_\psi^2}{2}} d\Delta\psi_k, \quad (45)$$

Afterwards, by using the change-of-variable method in calcu-

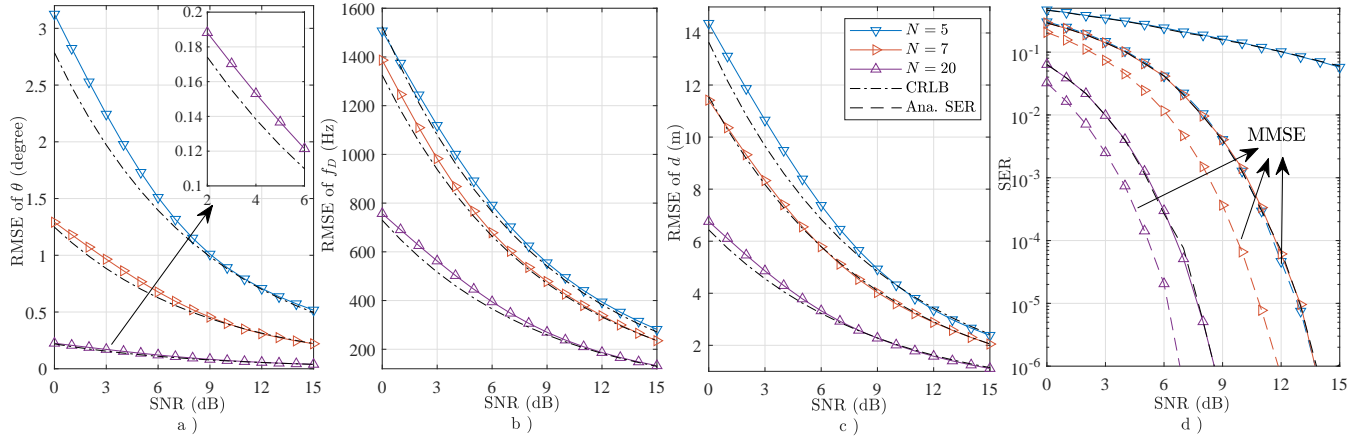


Fig. 8. The a) RMSE of DOA θ , b) RMSE of Doppler frequency f_D , c) RMSE of Range d , d) SER with the increase of SNR

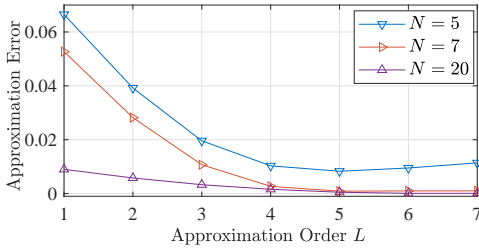


Fig. 9. The approximation performance with the increase of approximation order L .

lating integrals, I_ψ can be evaluated as

$$I_\psi = \frac{\sqrt{2\pi\sigma_\psi^2} e^{-\frac{c_{20}^2\sigma_\psi^2}{2}}}{2} \int_{u_{\min}}^{u_{\max}} \frac{2e^{-u^2}}{\sqrt{\pi}} du \quad (46)$$

$$= \frac{\sqrt{2\pi\sigma_\psi^2} e^{-\frac{c_{20}^2\sigma_\psi^2}{2}} [\text{erf}(u_{\max}) - \text{erf}(u_{\min})]}{2},$$

where $u = \frac{\sqrt{2}\Delta\psi_k \mp j\sqrt{2}C_{20}\sigma_\psi^2}{2\sigma_\psi}$. As a consequence, $u_{\max} = \frac{\sqrt{2}\Delta\psi_{\max} \mp j\sqrt{2}C_{20}\sigma_\psi^2}{2\sigma_\psi}$ and $u_{\min} = \frac{\sqrt{2}\Delta\psi_{\min} \mp j\sqrt{2}C_{20}\sigma_\psi^2}{2\sigma_\psi}$.

REFERENCES

- [1] Z. Wang, X. Mu and Y. Liu, "STARS enabled integrated sensing and communications," *IEEE Trans. Wireless Commun.*, doi: 10.1109/TWC.2023.3245297.
- [2] H. Zhang, *et al.*, "Holographic integrated sensing and communication," *IEEE J. Sel. Topics Signal Process.*, vol. 40, no. 7, pp. 2114-2130, July 2022.
- [3] C. Ouyang, Y. Liu and H. Yang, "Performance of downlink and uplink integrated sensing and communications (ISAC) systems," *IEEE Wireless Commun. Lett.*, vol. 11, no. 9, pp. 1850-1854, Sept. 2022.
- [4] C. Ouyang, Y. Liu and H. Yang, "Fundamental detection probability vs. achievable rate tradeoff in integrated sensing and communication systems," *IEEE Trans. Wireless Commun.*, vol. 22, no. 12, pp. 9835-9853, Dec. 2023.
- [5] H. Hua, T. X. Han and J. Xu, "MIMO integrated sensing and communication: CRB-rate tradeoff," *IEEE Trans. Wireless Commun.*, vol. 23, no. 4, pp. 2839-2854, April 2024.
- [6] D. Grgnođlu, E. Bjrnmson and G. Fodor, "Joint pilot-based localization and channel estimation in RIS-aided communication systems," *IEEE Wireless Commun. Lett.*, doi: 10.1109/LWC.2024.3454370.
- [7] C. Ouyang, Y. Liu and H. Yang, "On the performance of uplink ISAC systems," *IEEE Commun. Lett.*, vol. 26, no. 8, pp. 1769-1773, Aug. 2022.
- [8] W. Yuan, *et al.*, "Integrated sensing and communication-assisted orthog-
- onal time frequency space transmission for vehicular networks," *IEEE J. Sel. Topics Signal Process.*, vol. 15, no. 6, pp. 1515-1528, Nov. 2021.
- [9] Z. Wang, *et al.*, "NOMA empowered integrated sensing and communication," *IEEE Commun. Lett.*, vol. 26, no. 3, pp. 677-681, March 2022.
- [10] Z. Lyu, G. Zhu and J. Xu, "Joint manoeuvr and beamforming design for UAV-enabled integrated sensing and communication," *IEEE Trans. Wireless Commun.*, vol. 22, no. 4, pp. 2424-2440, April 2023.
- [11] C. Dou, *et al.*, "Sensing-efficient NOMA-aided integrated sensing and communication: a joint sensing scheduling and beamforming optimization," *IEEE Trans. Veh. Technol.*, vol. 72, no. 10, pp. 13591-13603, Oct. 2023.
- [12] K. Meng, *et al.*, "Throughput maximization for UAV-enabled integrated periodic sensing and communication," *IEEE Trans. Wireless Commun.*, vol. 22, no. 1, pp. 671-687, Jan. 2023.
- [13] Z. Wang, *et al.*, "Multi-vehicle tracking and ID association based on integrated sensing and communication signaling," *IEEE Wireless Commun. Lett.*, vol. 11, no. 9, pp. 1960-1964, Sept. 2022.
- [14] Y. Xiong, *et al.*, "On the fundamental tradeoff of integrated sensing and communications under gaussian channels," *IEEE Trans. Inf. Theory*, vol. 69, no. 9, pp. 5723-5751, Sept. 2023.
- [15] X. Li, S. Guo, T. Li, X. Zou and D. Li, "On the performance trade-off of distributed integrated sensing and communication networks," *IEEE Wireless Commun. Lett.*, vol. 12, no. 12, pp. 2033-2037, Dec. 2023.
- [16] H. Li, "Dual function trade-off in joint communications and radar: an electromagnetic field analysis," *Proc. Global Telecommun. Conf.*, 2021, pp. 1-6.
- [17] Z. Gao, *et al.*, "Integrated sensing and communication with mmWave massive MIMO: A compressed sampling perspective," *IEEE Trans. Wireless Commun.*, vol. 22, no. 3, pp. 1745-1762, March 2023.
- [18] Z. Huang, *et al.*, "Joint pilot optimization, target detection and channel estimation for integrated sensing and communication systems," *IEEE Trans. Wireless Commun.*, vol. 21, no. 12, pp. 10351-10365, Dec. 2022.
- [19] Y. Jiang, *et al.*, "UAV-enabled integrated sensing and communication: tracking design and optimization," *IEEE Commun. Lett.*, vol. 28, no. 5, pp. 1024-1028, May 2024.
- [20] J. Wu, W. Yuan and L. Bai, "On the interplay between sensing and communications for UAV trajectory design," *IEEE IoT J.*, vol. 10, no. 23, pp. 20383-20395, 1 Dec.1, 20233.
- [21] Q. Zhang, *et al.*, "Power scaling of uplink massive MIMO systems with arbitrary-rank channel means," *IEEE J. Sel. Topics Signal Process.*, vol. 8, no. 5, pp. 966-981, Oct. 2014.
- [22] P. Liu, *et al.*, "Channel estimation aware performance analysis for massive MIMO with rician fading," *IEEE Trans. Commun.*, vol. 69, no. 7, pp. 4373-4386, July 2021.
- [23] S. Misra *et al.*, "Cooperative localization of a GPS-denied UAV using direction-of-arrival measurements," *IEEE Trans. Aerosp. Electron. Syst.*, vol. 56, no. 3, pp. 1966-1978, Jun. 2020.
- [24] L. Zheng *et al.*, "Detection of ghost targets for automotive radar in the presence of multipath," *IEEE Trans. Signal Process.*, vol. 72, pp. 2204-2220, 2024.
- [25] Z. Yun and M. F. Iskander, "Ray tracing for radio propagation modeling: principles and applications," *IEEE Access*, vol. 3, pp. 1089-1100, 2015.
- [26] Z. Gao *et al.*, "Integrated sensing and communication with mmWave

- massive MIMO: A compressed sampling perspective," *IEEE Trans. Wireless Commun.*, vol. 22, no. 3, pp. 1745-1762, March 2023.
- [27] T. Van Chien *et al.*, "Joint computation offloading and target tracking in integrated sensing and communication enabled UAV networks," *IEEE Commun. Lett.*, vol. 28, no. 6, pp. 1327-1331, June 2024.
- [28] S. M. Kay, *Fundamentals of Statistical Signal Processing: Estimation Theory*. vol. 2. Cliffs, NJ, USA: Prentice-Hall, 1998.